Biosensors and Bioelectronics 156 (2020) 112095

Contents lists available at ScienceDirect

Biosensors and Bioelectronics

journal homepage: http://www.elsevier.com/locate/bios

Smartphone-assisted robust enzymes@MOFs-based paper biosensor for point-of-care detection

Xiaoxue Kou [a], Linjing Tong [a], Yujian Shen [a], Wangshu Zhu [b], Li Yin [a], Siming Huang [b,*], Fang Zhu [a,**], Guosheng Chen [a,***], Gangfeng Ouyang [a]

[a] MOE Key Laboratory of Bioinorganic and Synthetic Chemistry, School of Chemistry, Sun Yat-sen University, Guangzhou, 510275, China
[b] Department of Radiology, Sun Yat-sen Memorial Hospital, Sun Yat-sen University, Guangzhou, 510120, China

ARTICLE INFO

Keywords:
Point-of-care detection
Biosensor
Enzyme immobilization
Metal-organic frameworks
Smartphone detection

ABSTRACT:

Portable devices featured with fast analysis and affordable methodologies for clinical diagnostics have stimulated the rapid development of point-of-care (POC) technologies, potentially lowering the mortality rate. Herein, we demonstrated a portable, robust, and user-friendly intelligent metal-organic frameworks (MOFs) paper device, called smartphone-assisted biomimetic MOFs nanoreactor colorimetric paper (SBMCP), for on-demand POC detection of endogenous biomolecules. The concept of this paper platform was analogous to the intracellular cascades signal transduction, wherein the single/multiple enzymes components trapped within a ZIF-8 exoskeleton allowed the sensitive and selective recognition of target analyte *via* the accessible micropores network of ZIF-8, and then transferred the recognition event to a visual color signal based on the cascade reaction. Meanwhile, the ZIF-8 exoskeleton also endowed the enzymes with significantly elevated stability. As a result, this robust and portable SBMCP sensor enabled the on-site analysis of different important disease-related biomolecules through modulating the enzyme cascades, combining with a custom-designed smartphone application for signal readout. In the SBMCP assay, no sophisticated instruments or professional skill of the user was required, only 5 μL sample volume was needed, and the whole analysis process could be achieved within a portable MOFs paper and pervasive smartphone, endowing this new assay with the merits of low-cost, time-saving and easy-to-use. We demonstrated this SBMCP sensor was capable of real-time colorimetric detection of glucose and uric acid in diabetes and gout events. It is believed that this portable biosensor platform proposed herein potentially represents promising alternatives for POC diagnosis, especially applicable in developing world and resource-limited settings.

1. Introduction

Daily, point-of-care (POC) devices in the field of modern diagnostics offer the possibility of rapid, on-site and cost effective outcomes at patient's location in a variety of environments without requiring sophisticated laboratory infrastructure (Yu et al., 2018; Quesada-González and Merkoçi, 2018; Brangel et al., 2018). Especially for qualitative detection of disease-related biomolecules, the capability of POC technologies has the potential to streamline healthcare and early diagnosis, substantially carry out more timely intervention of metabolic disorders treatment (Kanchia et al., 2018; Zhu et al., 2014; Zarei, 2017). However, due to their poor abundance in complex biological matrix, especially at earlier stages of diseases, ideal analytical platform applicable to multiple biomolecules shows great potential in future biomedical solutions.

At present, traditional diagnostics of disease-related biomolecules are normally carried out using enzyme-linked immunosorbent assays (ELISAs) in suitably equipped laboratories (Rissin et al., 2010; Chen et al., 2018a; Xianyu et al., 2014). Many lab-based ELISAs have been developed for POC immunoassays, including the use of volumetric bar-chart chips for the naked-eye detection of cancer biomarkers (Li et al., 2016; Chen et al., 2018b), employment of gas-generation reaction as pressure-based signaling strategy to measure prostate specific antigen (Zhu et al., 2015), and application of graphene oxidecoated nanopaper for multiplex detection of pathogen and human protein

* Corresponding author.
** Corresponding author.
*** Corresponding author.
E-mail addresses: huangsm35@mail.sysu.edu.cn (S. Huang), ceszhuf@mail.sysu.edu.cn (F. Zhu), chengsh39@mail.sysu.edu.cn (G. Chen).

https://doi.org/10.1016/j.bios.2020.112095
Received 26 December 2019; Received in revised form 1 February 2020; Accepted 12 February 2020
Available online 20 February 2020

(Cheeveewattanagul et al., 2017). Despite their importance, the majority of these ELISAs rely on enzymes, antibodies and DNA for specific recognition. However, these bioactive recognition elements often display fragile nature such as low stability upon external stimuli, and inevitable purification steps cause inaccurate outcomes and short service life. In addition, the requirement of costly instruments and professional operation skills also hindered the POC immunoassays for broader use in clinical settings.

Enzyme immobilization is one of the key strategies for improving the fragile nature of the enzymes, which also offers effective control of the reaction processes and facile separation from the reaction system (Zhou and Hartmann, 2013). Over the past few decades, porous inorganic materials such as mesoporous silica, sol-gel matrices and carbon materials have been developed as competitive supports for enzyme immobilization. Nevertheless, substantial challenges, including low loading efficiency, incompact confinement, and the restricted pore size of the supports, are still remained. *In-situ* enzymes encapsulated within metal-organic frameworks (enzymes@MOFs) is an innovative biomimetic immobilization strategy that enabling to circumvent the aforementioned limitations of the immobilization by inorganic materials, because: 1) the ultrahigh porosity of MOFs provides sufficient space for hosting biomicromolecules; 2) the tightly packed enzymes protected by MOFs layer through conformational confinement enables to significantly elevate their stability; 3) it allows to *in-situ* encapsulate enzymes within MOFs that possessed significantly smaller pores than enzymes themselves (Huang et al., 2020). Initial studies by our group and others have demonstrated the enzymes@MOFs could not only improve the stability of the encapsulated enzymes through the structural confinement, but also allow the selective mass transfer of the guest *via* the accessible micropores network of the MOFs exoskeleton (Chen et al. 2019, 2020; Lian et al., 2017; Doonan et al., 2017; Feng et al., 2019). This MOFs immobilization technique may pay the way for rational design of robust POC sensor, yet not reported.

Cellulose paper with the attractive properties of high mechanical strength and fexibility, abundant porosity and broad chemical-modification capabilities is known for the ideal substrate for POC devices (Morales-Narvá ez et al., 2015). A mobile phone contains all vital components required for a common analytical readout including the controllable screen and an signal input *via* the camera (Yetisen et al., 2019; Mahato and Chandra, 2019). With these considerations in mind, we herein reported a smartphone-assisted biomimetic MOFs nanoreactor colorimetric paper (SBMCP) device, enabling to realize facile

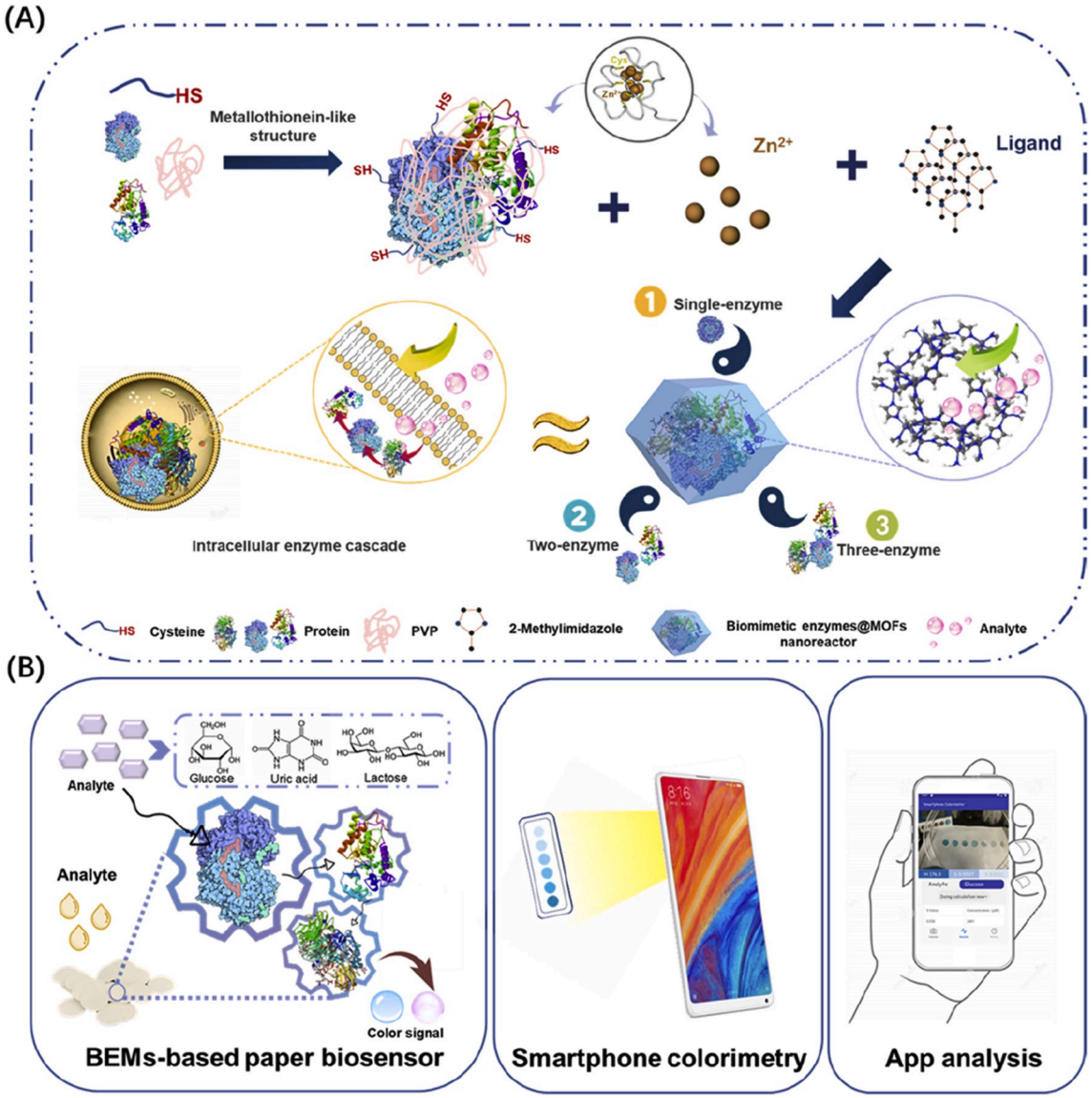

Scheme 1. (A) Synthesis routes of the biomimetic enzymes@MOFs (BEMs) based on the formation of the mercaptide bonds (left) and the self-assembly amino-boosted biomineralization approach. (B) Schematic representation of smartphone-assisted robust enzymes@MOFs colorimetry strategy.

POC detection. Single enzyme or multiple enzymes system was *in situ* encapsulated within ZIF-8 through an amino acid-boosted biomimetic mineralization, and then a MOFs paper was prepared by a direct loading approach. The concept of this paper platform was analogous to the intracellular enzyme cascades event (Scheme 1A), wherein the enzymes components trapped within a biomineralized ZIF-8 exoskeleton allowed the sensitive and selective recognition of target analyte *via* the accessible micropores network of ZIF-8, and then transfered the recognition event to a visual color signal based on the cascade reaction, which was feasible to real-time and *in-situ* readout by a custom-designed smartphone application (App) (Scheme 1B). We demonstrated that the protective ZIF-8 layer endowed the POC sensor with significantly elevated stability and improved condition tolerance. Improtantly, this new SBMCP was facile to realize on-demand POC sensing of different disease-related biomolecules (glucose, uric acid, lactose, urea, etc.) through modulating the enzymes components. Additionally, real-time POC detection of glucose and uric acid in diabetes and gout events was achieved using this SBMCP. This approach overcomes the drawbacks of conventional immunoassays and possessed the merits of high stability, cost-efficient, and enables to on-site analysis. We are confident that this low-cost and easy-to-use MOFs paper will become a promising alternative for POC detection.

2. Experimental Section

2.1. Reagents and apparatus

Full details are given in the Supportion Information section.

2.2. Synthesis of the biomimetic enzymes@MOFs nanoreactor

Synthesis of the biomimetic enzymes@MOFs (BEMs) was carried out according to our previously reported procedure with slight changes (Chen et al., 2019). In a typical amino acid-boosted biomineralization process, for single enzyme entrapped, 0.5 mg urease were firstly added in 2 mL 2-methylimidazole (800 mM, pH = 10.5) in a 5 mL vial, followed by adding 2 mg PVP (MW: 8000) and stirred for 1 min. Then 0.5 mg Cys was introduced and the solution was stirred for 3 min. Finally, 2 mL zinc acetate solution (80 mM) was added and aged at room temperature for 4 h. For two enzymes entrapped, 0.5 mg oxidase and 0.5 mg HRP were firstly added in 2 mL 2-methylimidazole (800 mM, pH = 10.5) in a 5 mL vial, followed by adding 2 mg PVP (MW: 8000) and stirred for 1 min. Then 2 mg Cys was introduced GOx/HRP system and UOx/HRP system. The solution was then stirred for 3 min. Finally, 2 mL zinc acetate solution (80 mM) was added and aged at room temperature for 4 h. For multiple enzymes entrapped, 1.0 mg β-Gal, 0.5 mg oxidase and 0.5 mg HRP were firstly added in 2 mL 2-methylimidazole (400 mM, pH = 10.5) in a 5 mL vial, followed by adding 2 mg PVP (MW: 8000) and stirred for 1 min. Then 2 mg Cys was introduced the solution was stirred for 3 min. Finally, 2 mL zinc acetate solution (40 mM) was added and aged at room temperature for 2 h.

2.3. Fabrication of smartphone-assisted biomimetic MOFs colorimetric paper

Paper cutting is a low-cost approach for the manufacture of paper-based POC devices due to its high time efficiency and batch production potential. Briefly, the raw paper were crafted into a round zone with diameter 6 mm by office paper perforator, followed by washing with water to remove unwanted impurities. 2 mg BEMs were dispersed in 250 μL 1% PVA solution to form a BEMs sticky solution. In the direct loading approach, 5 μL aforementioned BEMs sticky solution was carefully dropped onto the raw round paper and then dried at room temperature. The detailed schematic representation of fabrication process and principle involved in signal generation were shown in Fig. 2A.

The custom-designed smartphones App was developed in Java language on a popular integrated development environment (IDE) for Android development, which called Android Studio. The biosensing experiments were carried out in fume hood and a light-emitting diode (LED) light was fixed on the smartphone (Fig. S13) for ensuring the stability of environmental light condition. In addition, an approximate focal length between the MOFs paper and smartphone was fixed to improve the accuracy. The flow chart of this HSV-App was shown in Fig. S14. The main interface of this App includes two mode called color scan and photo album. First, the image of the MOFs paper was collected using the smartphone camera upon touching the button of Camera, while the LED was turned on. In the other mode, images could be directly loaded from smartphone album when choosing the button of History. Then, the Red-Green-Blue (RGB) values of each pixel from the touchscreen area were obtained and converted into HSV values through the matrix transformation algorithm. With regard to the calibration model between the saturation value of the image and the concentration of the analyte, the linear fitting equation was obtained, and these linear calibration curves for different analytes were then imported in this HSV-App. After that, the concentration of analyte was feasible to output based on SBMCP.

2.4. SBMCP for disease-related biomolecules assay

In a typical SBMCP assay, 5 μL biological endogenous biomolecule stock solution or genuine sample was drop-casted onto the detection zone of the paper biosensor, followed by adding the 5 μL peroxidase substrate (TMB) to produce visual color singal. After incubation for a certain time, the visual color induced by target analyte was captured by smartphone camera. The photography was then analyzed by the self-developed App based on Android system. The target analyte induced colorimetric changes (Δ intensity) was calculated as follow:

$$\Delta\ Intensity\ =\ \left[\left(S_{sample}-S_{control}\right)\ \times\ 100\ \%\right. \quad (1)$$

where $S_{control}$ is the signal from blank paper biosensor with TMB only, S_{sample} is the average saturation value of paper biosensor after sample testing.

3. Results and discussion

3.1. Fabrication and characterization of biomimetic enzymes@MOFs nanoreactor

In order to overcome the intrinsic instability of enzyme-assisted recognition, we appareled the enzyme with an “armour-like” MOFs exoskeleton *via* self-assembly biomimetic mineralization under mild conditions. This artificial protective coating, crystalline solid-state MOFs, was *in-situ* grown around the enzymes through the well-established amino-boosted biomineralization approach with modification (Chen et al., 2019). The chief reason why zeolite imidazolate framework (ZIF-8) was chosen as exoskeleton for enzyme immobilization in our approach, was it exhibited excellent ability to accommodate a broad range of guests (e.g., amino acids, nanoparticles, enzymes, biopharmaceuticals etc.). When compared with the complicated synthesis process of other MOFs, ZIF-8 possessed a milder synthesis condition through incubation or stirring in room temperature. In this study, the enzymes components, polyvinylpyrrolidone (PVP) and cysteine (Cys) firstly self-assembled into a metallothionein-like structure that accelerating pre-nucleation of ZIF-8 and engendering MOFs formation around the enzyme (Palmiter, 1998; Peroza et al., 2009; Chen et al., 2019). The procedure for the fabrication of this biomimetic enzymes@MOFs (BEMs) was shown in Scheme 1A and full details were given in the Experimental Section.

We firstly chose two enzymes, glucose oxidase (GOx) and horseradish peroxidase (HRP), as the prototype enzyme pair, and entrapped them within ZIF-8 (GH-BEMs) to construct the robust glucose sensing

unit. The as-synthesized GH-BEMs displayed different colors compared to pure ZIF-8 due to the incorporation of the enzymes (Fig. S1A). As revealed in the scanning electron microscope (SEM) images of the resulting GH-BEMs (Fig. 1A), standard regular polyhedron structures as pure ZIF-8 (Fig. S1B) were formed which exhibited the diameters of 2–2.5 μm in average. The transmission electron microscopy (TEM) image also confirmed that GH-BEMs had the same morphology as pure ZIF-8 (Fig. 1B). Additionally, the existence and relatively uniform distribution of Fe element contributed to the heme groups of HRP (Ohlsson et al., 1977) was shown in the energy dispersive X-ray spectroscopy (EDS) mapping of GH-BEMs (Fig. 1C), demonstrating the HRP was indeed embedded in ZIF-8. And by comparing the powder X-ray diffraction (PXRD) between GH-BEMs and pure ZIF-8, the Bragg diffraction pattern was overlapped (Fig. 1D). It indicated that the crystal structure of GH-BEMs was not affected by the incorporation of the enzymes, which well agreed with the results of the SEM images.

To further confirm the entrapment of the enzymes pair within ZIF-8, the confocal laser scanning microscopy imaging of GOx and HRP in ZIF-8, wherein the Gox and HRP were priored to be labeled with fluorescein isothiocyanate (FITC) and rhodamine B (RhB) respectively, revealed that both enzymes were homogenously incorporated within the MOFs (Fig. 1E). The remained protein in the supernatant after synthesis was measured by fluorescence spectrometer. As anticipated, no FITC-GOx or RhB-HRP was detected (Fig. S2). This result demonstrated that almost all of the enzymes were encapsulated in ZIF-8. And the encapsulated efficiency was as high as ca. 99.1% and ca. 91.0% for GOx and HRP, respectively.

Further characterization of GH-BEMs was performed using Fourier-transform infrared (FT-IR) measurements. The presence of two enzymes in ZIF-8 produced new FT-IR peaks (Fig. S3) ranging from ~1640–1660 cm^{-1} and ~1550–1570 cm^{-1}, corresponding to the vibration peaks of amide I and amide II, respectively. These characteristic vibrations suggested that the enzymes maintain their natural secondary structure (Patra et al., 2015) after mild biomineralization condition within ZIF-8. Next, as depicted in Fig. S4, the result of thermal gravity analysis (TGA) well supported the incorperation of enzyme within ZIF-8. During the decomposition stage around 250 °C–500 °C, the GH-BEMs composite had much more weight loss than the pure ZIF-8 crystals, which could be attributed to the decomposition of embedded enzymes. Additionally, nitrogen adsorption analysis shown that GH-BEMs actually inherited the porous structure of ZIF-8. Meanwhile, the reduced surface area from 2083 m^2/g to 1393 m^2/g compared with the pure ZIF-8 well supported the encapsulated of the enzymes (Fig. S5). These together data demonstrated that the ZIF 8-encapsulated enzymes structure was indeed formed.

We next confirmed the enzyme-cascade within the GH-BEMs. The enzyme-cascade mechanism was shown in Fig. S6A. Briefly, in the presence of glucose as a substrate, the aerobic GOx-biocatalyzed oxidation of glucose yields gluconic acid and H_2O_2, and the cascade HRP-biocatalysis occurred based on the generated H_2O_2 when using 3,3′,5,5′-tetramethylbenzidine (TMB) as a substrate. The product of the enzyme-cascade (Abs at 650 nm) was monitorable in the GH-BEMs, indicating the enzyme-cascade process indeed occurred. As a comparsion, no signal was detected in the control experiments, which replacing the GH-BEMs with pure ZIF-8 or single enzyme-encapsulated ZIF-8 (Fig. S6B). These results verified that the guest was feasible to diffuse into the MOFs *via* the accessible micropores network, and activated the enzyme-cascade.

3.2. Smartphone-assisted biomimetic MOFs colorimetric paper

Cellulose paper was chosen as an ideal substrate for constructing the

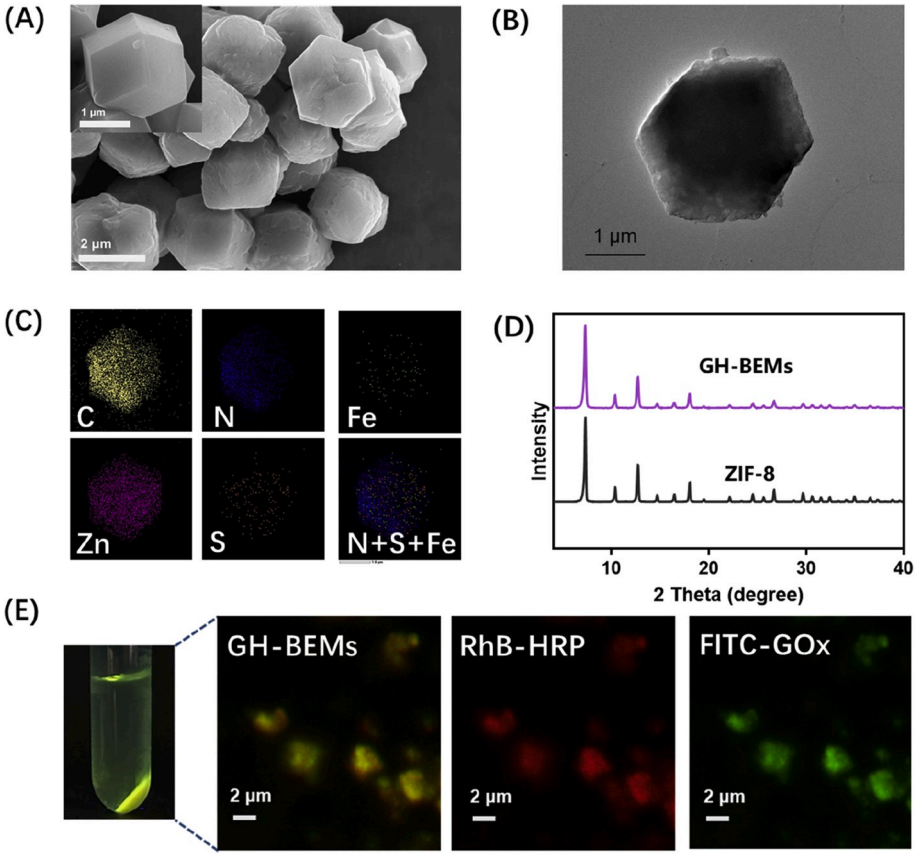

Fig. 1. (A) SEM imaging of the GH-BEMs and the magnified image (the insert). (B) TEM imaging of the GH-BEMs. (C) The corresponding elemental mapping of the GH-BEMs. (D) The PXRD patterns of the GH-BEMs and pure ZIF-8. (E) The confocal laser scanning microscopy image of the GH-BEMs.

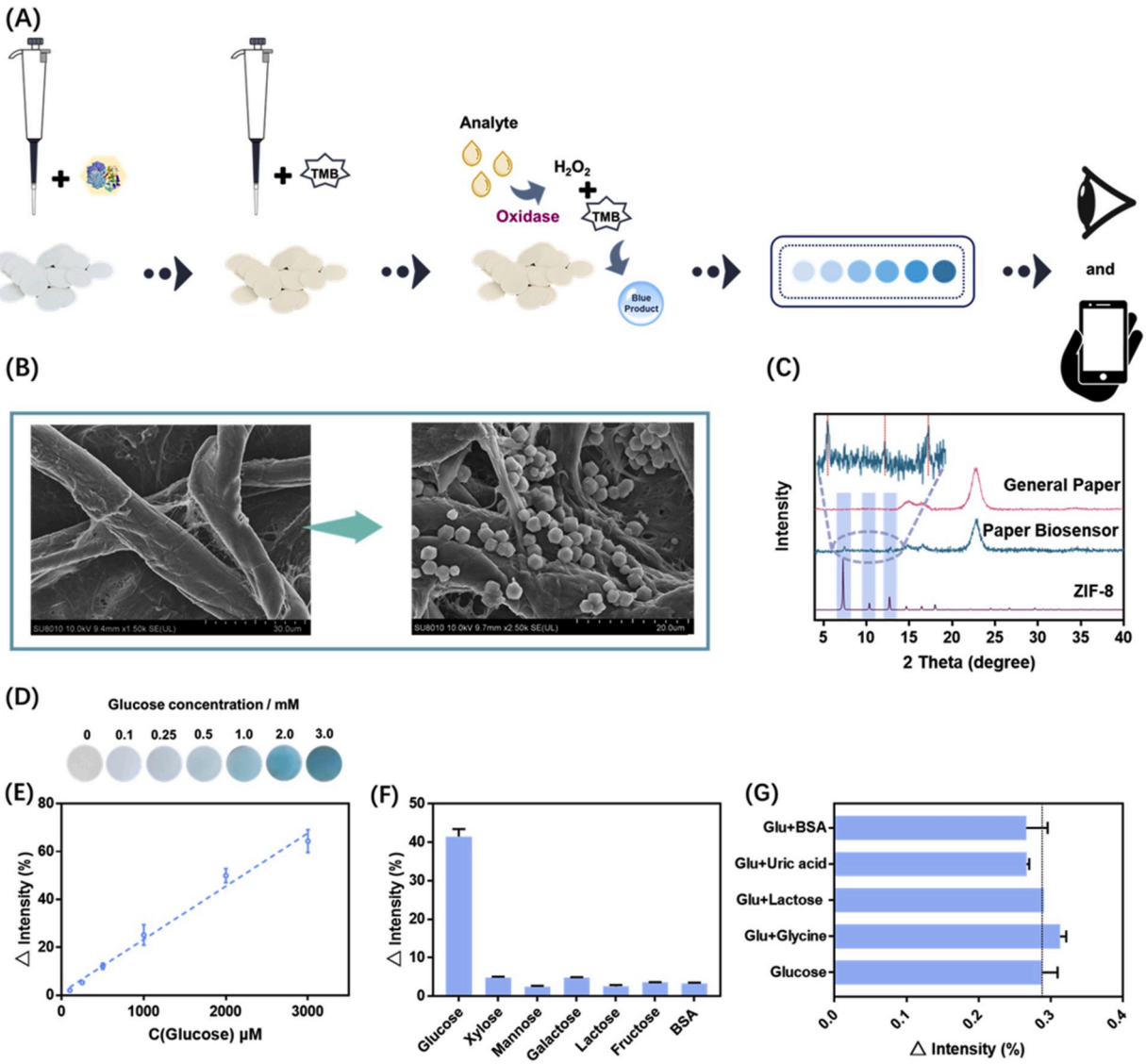

Fig. 2. (A) Schematic illustration for the enzymes@MOFs-based paper biosensor colorimetic assay. (B) SEM images showing the morphology of the paper prior to (left) and after (right) GH-BEMs modification. (C) The PXRD patterns of the general paper, GH-BEMs paper biosensor and pure ZIF-8. (D) Digital images of the GH-BEMs paper biosensors in the presence of different concentrations of glucose in PBS solution. (E) Analytical curves for glucose detection with dependence the intensity of S value at the MOFs paper biosensors. (F) Interference test of the SBMCP toward glucose detection. Sample: 2 mM glucose or 4 mM interfering saccharides or 1 mg mL^{-1} protein in PBS solution. (G) Cross-reactivity test of the SBMCP toward glucose detection. Sample: 1.25 mM glucose and equal interfering substances in PBS solution.

BEMs paper becasuse of its inexpensive cost, abundant porosity and broad chemical-modification capability. The prepared GH-BEMs were firstly dispersed in polyvinyl alcohol (PVA), and the mixture was directly loaded onto the cellulose paper to form BEMs sensing paper (Fig. 2A). The PVA was used herein for two considerations: 1) PVA can serve as the dispersant and agglutinant that enabling to uniformly fix the BEMs onto the cellulose paper; 2) The paper surface modified with PVA was capable of improving the homogeneity on color measurements that compromise the sensitivity and detectability levels in clinical diagnosis (Zhao et al., 2008). The SEM imaging of the obtained BEMs paper biosensor indicated the porous cellulose paper surface was uniformly coated with GH-BEMs (Fig. 2B), favouring the homogeneity on transformed color signal measurements (Figueredo et al., 2016). The PXRD tests were also conducted to identify the ZIF-8 structure on the BEMs paper biosensor (Fig. 2C), and the three distinct peaks, assigning to (110), (200), (211) orientations of ZIF-8, were recorded, respectively. These results well confirmed that the GH-BEMs sensing paper was successfully prepared.

The evaluations of the color changes by the naked eyes normally lack of certainty due to differences in personal perception, even with a corresponding color chart. This restriction becomes major hurdle for colorimetric POC devices. In fact, an all-pervading smartphone already exhibits excellent color recognition ability based on the Red-Green-Blue (RGB) color model. The smartphone device also contains other vital components required for analytical readout including the controllable screen and high-resolution camera. With these in minds, we sought to develop a smartphone-assisted biomimetic MOFs nanoreactor colorimetric paper (SBMCP).

We firstly designed a smartphone App with Hue-Saturation-Value (HSV) values recording ability (HSV-App), enabling to provide a real-time readout for SBMCP (Fig. S7, details seen in the Experimental Section). Diabetes mellitus is a kind of metabolic dysfunction with abrupt variations of glucose concentration. The mean glucose concentration higher than 7.0 mM may be an early on-set of diabetes (Wasserman, 2009). As a proof of concept, the feasibility of the proposed SBMCP for POC detection of glucose was evaluated. The perfomance of SBMCP was

investigated in terms of the linearity, sensitivity and specifity. As shown in Fig. 2D, the color of the GH-BEMs paper gradually changed from white to shiny blue when a small amount of glucose standard solution (only need 5 μL) was dropped onto the paper surface. In addition, the color signal reached a saturation point within 9 min (Fig. S8). Such high-speed signal readout was atrributed to high-efficiency catalytic cascades process at the intercommunicating enzymes encapsulated within MOFs. As a comparsion, the conventional enzyme-linked diagnostic assays usually take more than 30 min for visual readout. The merits of extremely small sample volume requirements and fast speed readout endow BEMs paper with great potential for POC detection.

The color signal was then recognized by the high-resolution camera, and treated by the established HSV-App. Excellent linear relationship was observed between the corresponding saturation value (S) obtained from HSV-App and the concentration (C) of glucose ranging from 100 μM to 3000 μM, which could be described by Δ Intensity = 0.0222 × C + 1.149 (R^2 = 0.9883) (Fig. 2E). The lowest detectable concentration of glucose with naked-eyes was 250 μM, which was comparable to those reported in other state-of-art colorimetric methods (Table S1, Supporting Information). In addition, the spiked recoveries for glucose in standard solution were ranged from 98.2% to 108.4%, indicating the desirable accuracy of the SBMCP (Table S2).

We next evaluated the specifity of the SBMCP toward glucose. Several biomolecules including xylose, mannose, galactose, lactose, fructose and albmin were used as the interferant. As shown in Fig. 2F, glucose yielded a significantly high color signal in the SBMCP assay. In contrast, no color change was observed in those interferants tests, in spite that all of them were at 2-times higher concentrations than glucose. Moreover, the cross-reactivity of SBMCP biosensor toward different interferences was also evaluated, and the calculated values ranged from 1.0% to 8.9%, which was acceptable for biological analysis (Fig. 2G). All of these results demonstrated that the whole assay including recognization, signal transduction and readout could be rapidly completed in the designed SBMCP, with excellent linearity, sensitivity and specifity.

3.3. The enhanced stability and life-time for POC detection

The capacity to withstand changes in external conditions is extremely important for robust POC devices. For enzyme-based POC devices, the digestive enzymes-caused degradation and unfolding structure per se are two major reasons related to the poor stability of enzyme, in which the free enzyme may lose its biological functions. In nature, the self-triggered biomineralization can closely cover on the soft tissues, thereby producing a robust protective layer against the harsh surroundings. Enlightened by this natural phenomenon, the mineralized ZIF-8 protective layer, which was analogous to the natural biomineraliztion layer, may endow the BEMs with high stability under denaturing conditions.

Protease is a kind of biomacromolecule that can devitalize the enzymes through hydrolysis, and widely exist in biofluid. Therefore, enzymes-based POC devices gave risks to be invalid for biofluid analysis. We firstly evaluated the protecting effect of the robust MOFs layer against protease-triggered hydrolysis. Through size-selective channel, the microporous scaffold of ZIF-8 could exclude trypsin, and thus prevent the cascade system from hydrolysis. It could be seen in Fig. 4A, the bioactivity of GH-BEMs remained 74.1% while that of the two free enzymes in homogeneous solution decreased to 22.2%, confirming the excellent shielding function of the robustness of ZIF-8 layer. Besides, the denaturant-induced or heat-induced unfolding are other common risks that could denature the enzyme. Urea is a typical chaotropic chemical capable of disrupting the interior hydrogen bond of proteins, leading to the unfolding of proteins (Liao et al., 2017). Similarly, the GH-BEMs in the presence of 6 M urea retained 89.5% of its original bioactivity, whereas the two free enzymes retained very low bioactivity after urea treatment (Fig. 3A). Furthermore, the GH-BEMs still remained high bioactivities even when exposing them to ethanol or high temperature (100 °C) (Fig. 3A). These results showed enhanced stability of GH-BEMs, attributing to the robust mineralized ZIF-8 layer that enabling to confine the structural conformation of the protein (Chen et al. 2019, 2020).

The long-term storage stability is an another important aspect for developing a reliable POC biosensor. As shown in Fig. 3B, the BEMs retained ca. 80% of initial overall activity for 4 weeks at room temperature, however, the two free enzymes in homogeneous solution almost lost their bioactivity in the same condition. Clearly, the significantly enhanced stablity and life-time of the emzymes@MOFs paper will allow SBMCP to operate in sophisticated applications.

3.4. On-demand POC detection through encapsulating different enzymes system

The POC device featuring on-demand detection function favoured for clinical diagnosis. This on-demand POC detection is also facile to be realized in our SBMCP assay *via* modulating the encapsulation of different enzymes system including single-enzyme, two-enzyme and even three-enzyme biocatalytic systems within MOFs paper (Fig. 4, the details for the fabrication were described in the Experimental Section).

For single-enzyme biocatalytic system, we encapsulated urease into the MOFs paper for POC detection of urea. Urease is normally used to catalyze the hydrolysis of urea into ammonia and carbon dioxide. The pH elevated by the reaction can be translated into a visual color signal with phenol red as an indicator. Based on this catalytic mechanism, we designed urease-entrapped biomimetic enzymes@MOFs (Urease-BEMs) paper (Figs. 4A and S9) and investigated its sensing possibility. A clear red color signal could be observed when dropping urease onto Urease-BEMs paper (Fig. 4A).

Uric acid has been routinely used as an important marker molecule in clinical determination for diseases associated with purine metabolism. Hyperuricemia assosicated with extremely high level of uric acid is linked with diseases as gout, kidney impairment, leukemia and others (Falasca, 2006; Raj and Ohsaka, 2003). We next encapsulated urate oxidase (UOx)-HRP two-enzyme biocatalytic systems within ZIF-8, named UH-BEMs, for POC detection of uric acid (Fig. 4B). The sensing mechanism of the UH-BEMs paper were described in Fig. 4B and Fig. S10. Based on the similar SBMCP assay, the corresponding S value exhibited a linear response toward uric acid concentration within the range of 0.4 mM–1 mM, which could be described by Δ Intensity = 13.23 × ln(C) + 19.68 (R^2 = 9886) (Figs. S11A and S11B). As of note, the limit for naked eye-visible readout was 0.5 mM, which well met the requirement for diagnosing uric acid-related diseases using plasma. Because the normal level of uric acid is within the range of 0.13–0.46 mM in serum (Luo et al., 2006). In addition, the spiked recovery tests were further conducted to evaluate the reliability of SBMCP. As summarized, recoveries for uric acid in standard solution were ranged from 103.1% to 106.3%, indicating the feasibility of the method for uric acid anlysis (Table S2). Furthermore, the specificity of UH-BEMs paper was confirmed using Arg, Cys, Glu, Glucose, BSA and TRF as interferants (Fig. S11C).

We further explored the possibility of three-enzyme system-entrapped biomimetic enzymes@MOFs paper for POC detection. As a proof of concept, β-galactosidase (β-Gal), GOx and HRP were coencapsulated within MOFs paper (named GGH-BEMs), aiming at the POC detection of lactose based on the triple cascade catalysis (Figs. 4C and S12). Excessive ingestion of lactose results in a host of physical symptoms such as diarrhoea, flatulence, explosive diarrhoea and cramps (Luyt et al., 2014). Therefore, the lactose monitoring in dairy products is of great importance in order to regulate the lactose uptake. The characterizations and sensing mechanism of the GGH-BEMs paper were described in Fig. 4C and Fig. S12. Based on the SBMCP assay, the corresponding S value exhibited a linear response toward lactose concentration within the range of 5 mM–120 mM, which could be described by Δ Intensity = 0.5717 × C – 2.223 (R^2 = 9963) (Figure S11D, S11E). The spiked recovery tests were further conducted to evaluate the reliability of SBMCP.

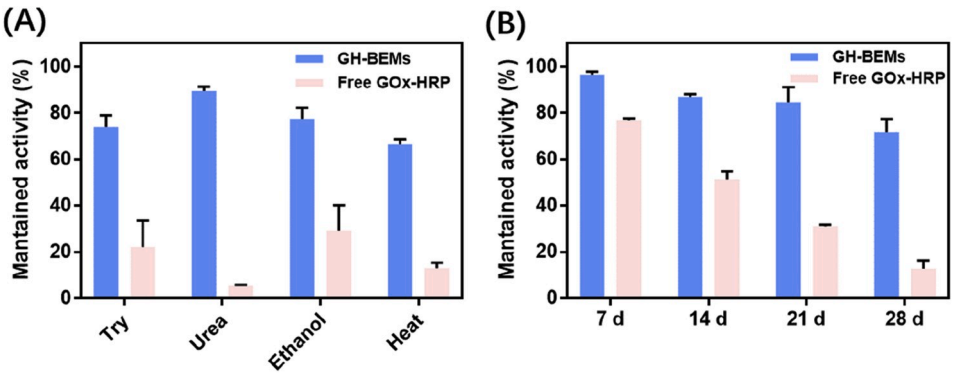

Fig. 3. The sensing performances of the GH-BEMs paper biosensor and free enzymes system after treated in the condition of 1 mg mL^{-1} trypin, 6 M urea or 100 °C for 30 min (A) and after keeping storage at room temperature for 7 d, 14 d, 21 d and 28 d (B).

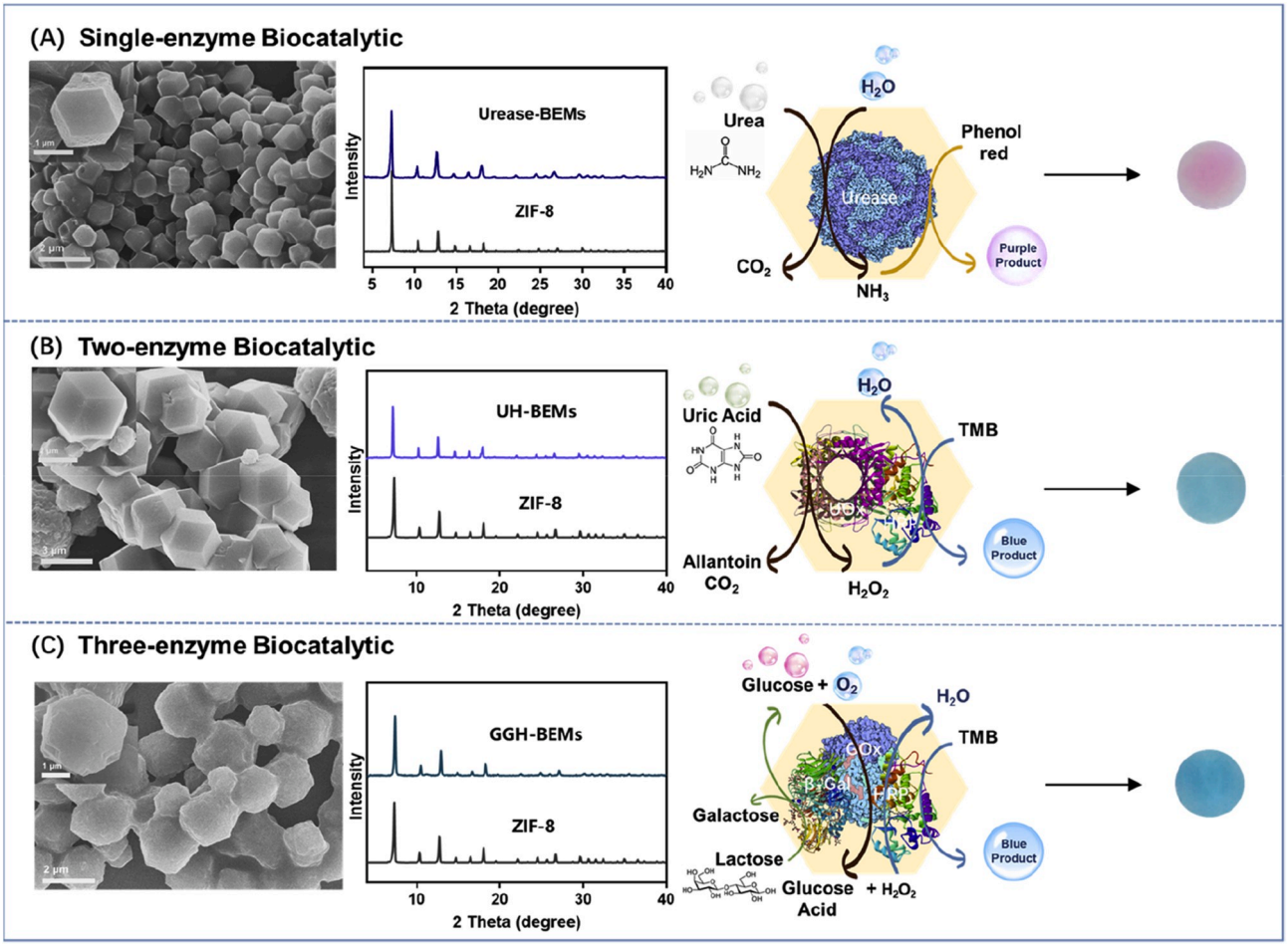

Fig. 4. The SEM images, XRD patterns, schematic representation of enzyme cascade reaction and sensing performace for urea, uric acid and lactose, respectively of single-enzyme (A) two-enzyme (B) and three-enzyme (C) biocatalytic systems.

As summarized, recoveries for lactose in standard solution were ranged from 99.67% to 107.3%, indicating the feasibility of our SBMCP for lactose POC detection (Table S2). Furthermore, the specificity of GGH-BEMs paper was confirmed using galactose, xylose, mannose, fructose, saccharose as interferants (Figure S11F).

3.5. Genuine sample analysis

The disequilibrium of various metabolic levels of disease-related biomolecules poses a severe threat to public health. The proved features of our SBMCP could potentially be applied as a rapid and on-site surveillance tool. We also envisioned that these advantages of SBMCP could provide an indispensable tool to streamline dignostics studies of metabolic disorders treatment for critical need. Using our SBMCP assay, real-time and on-site POC detection of glucose and uric acid in diabetes and gout events was achieved (Fig. 5). The signals yielded by human serum from diabetes patients were continously monitored in the 3 h after a meal. These obtained results suggested the existence of post-prandial hyperglycemia state, and could be determined by the naked eyes (Fig. 5A). Besides, the test results were broadly in line with those

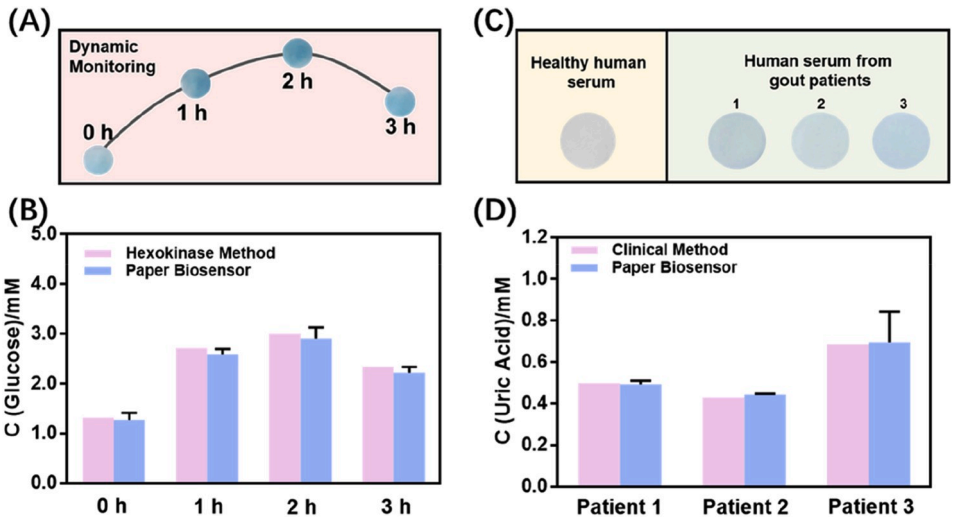

Fig. 5. (A) Photos of the GH-BEMs paper biosensors results from a diabetes patient serum before and after a meal during 3 h. (B) Glucose concentrations detected by SBMCP assay and hexokinas method in human serum from the above mentioned diabetic. (C) Photos of the UH-BEMs paper biosensors results in healthy human serum and human serum from gout patients. (D) Uric acid concentrations detected by SBMCP assay and clinical method in human serum from gout patients.

obtained by hexokinase method (Fig. 5B), but avoided cumbersome treatment and high cost. Furthermore, the signals yielded by human serum from gout patients were significantly higher than that yielded by healthy human serum, which also could facilely be distinguished by the naked eyes (Fig. 5C). In addition, the test results were in good agreement with those offered by clinical method (Fig. 5D), which in particular avoided tedious treatment and expensive charge. These findings demonstrated the SBMCP well satisfied the requirement for clinical applications.

4. Conclusion

POC diagnostic research aiming at on-site and real-time healthcare makes it appealing with the realization of rapid analysis and affordable methodologies in public use, especially in application scenarios with fewer resources. In this study, we developed an intriguing SBMCP assay enabling on-demand, rapid and sensitive detection of different disease-related biomolecules in a facile manner, by applying biomimetic enzymes@MOFs cascade system in tandem with an all-pervading smartphone. The MOFs exoskeleton-protected enzymes cascade paper biosensor presented the advantage with easy operation, remarkably elevated stability and tolerance as compared to the natural enzymes without protection.

Overall, the new SBMCP herein has addressed the critical need for facile and cost-efficient on-demand POC sensing of different endogenous disease-related biomolecules in a simple way. Although the disease-related biomolecules detection in human serum based SBMCP seems perfectly suited for on-site analysis in resource-constrained laboratories or countries, the invasive blood sampling and indispensable centrifugation step for blood sample processing may hinder it for broader use. As a noninvasive biological fluid, saliva and sweat are deemed as the future of POC real-life sample analysis. However, disease specific biomarkers present in very low abundance in noninvasive biological fluids. We anticipate the further improvement of the sensitivity will realize noninvasive biological fluid detection. On account of the ubiquitous smartphone, this low-cost and easy-to-use MOFs paper could potentially be a versatile analytical tool for POC diagnosis.

Declaration of competing interest

The authors declare that they have no known competing financial interests or personal relationships that could have appeared to influence the work reported in this paper.

CRediT authorship contribution statement

Xiaoxue Kou: Conceptualization, Methodology, Software, Investigation, Data curation, Writing - original draft. **Linjing Tong:** Investigation, Data curation. **Yujian Shen:** Software, Investigation. **Wangshu Zhu:** Resources. **Li Yin:** Software. **Siming Huang:** Data curation, Supervision. **Fang Zhu:** Supervision. **Guosheng Chen:** Supervision, Methodology, Data curation, Project administration, Funding acquisition. **Gangfeng Ouyang:** Supervision, Funding acquisition.

Acknowledgements

This research was supported by projects of National Natural Science Foundation of China 21904146, 21737006, 21677182 and 21527813), the project of Postdoctoral Innovative Talents Support Program (Boxin Plan, BX20190390), the project of China Postdoctoral Science Foundation (2019M653138) and Fundamental Research Funds for the Central Universities (19lgpy125).

Appendix A. Supplementary data

Supplementary data to this article can be found online at https://doi.org/10.1016/j.bios.2020.112095.

References

Quesada-González, D., Merkoçi, A., 2018. Chem. Soc. Rev. 47, 4697–4709.
Brangel, P., Sobarzo, A., Parolo, C., Miller, B.S., Howes, P.D., Gelkop, S., Lutwama, J.J., Dye, J.M., McKendry, R.A., Lobel, L., Stevens, M.M., 2018. ACS Nano 12, 63–73.
Cheeveewattanagul, N., Morales-Narváez, E., Hassan, A.-R.H.A., Bergua, J.F., Surareungchai, W., Somasundrum, M., Merkoçi, A., 2017. Adv. Funct. Mater. 27, 1702741.
Chen, C., Zhao, J., Lu, Y., Sun, J., Yang, X., 2018a. Anal. Chem. 90, 3505–3511.
Chen, G., Kou, X., Huang, S., Huang, S., Zhang, R., Liu, C., Shen, J., Zhu, F., Ouyang, G., 2018b. Adv. Funct. Mater. 28, 1804129.
Chen, G., Huang, S., Kou, X., Wei, S., Huang, S., Jiang, S., Shen, J., Zhu, F., Ouyang, G., 2019. Angew. Chem. Int. Ed. 58, 1463–1467.
Chen, G., Kou, X., Huang, S., Tong, L., Shen, Y., Zhu, W., Zhu, F., Ouyang, G., 2020. Angew. Chem. Int. Ed. 59, 2867–2874.
Doonan, C., Riccò, R., Liang, K., Bradshaw, D., Falcaro, P., 2017. Acc. Chem. Res. 50, 1423–1432.
Falasca, G.F., 2006. Clin. Dermatol. 24, 498–508.
Feng, Y., Wang, H., Zhang, S., Zhao, Y., Gao, J., Zheng, Y., Zhao, P., Zhang, Z., Zaworotko, M.J., Cheng, P., Ma, S., Chen, Y., 2019. Adv. Mater. 31, 1805148.

Figueredo, F., Garcia, P.T., Cortón, E., Coltro, W.K.T., 2016. ACS Appl. Mater. Interfaces 8, 11–15.
Huang, S., Kou, X., Shen, J., Chen, G., Ouyang, G., 2020. Angew. Chem. Int. Ed. https://doi.org/10.1002/anie.201916474, 2020.
Kanchia, S., Sabelaa, M.I., Mdlulia, P.S., Inamuddin, Bisettya, K., 2018. Biosens. Bioelectron. 102, 136–149.
Li, Y., Xuan, J., Song, Y., Qi, W., He, B., Wang, P., Qin, L., ACS Nano 10, 1640-1647.
Lian, X., Fang, Y., Joseph, E., Wang, Q., Li, J., Banerjee, S., Lollar, C., Wang, X., Zhou, H.-C., 2017. Chem. Soc. Rev. 46, 3386–3401.
Liao, F.-S., Lo, W.-S., Hsu, Y.-S., Wu, C.-C., Wang, S.-C., Shieh, F.-K., Morabito, J.V., Chou, L.-Y., Wu, K.C.-W., Tsung, C.-K., 2017. J. Am. Chem. Soc. 139, 6530–6533.
Luo, Y.-C., Do, J.-S., Liu, C.-C., 2006. Biosens. Bioelectron. 22, 482–488.
Luyt, D., Ball, H., Makwana, N., Green, M.R., Bravin, K., Nasser, S.M., Clark, A.T., 2014. Clin. Exp. Allergy 44, 642–672.
Mahato, K., Chandra, P., 2019. Biosens. Bioelectron. 128, 9–16.
Morales-Narvá ez, E., Golmohammadi, H., Naghdi, T., Yousefi, H., Kostiv, U., Horá k, D., Pourreza, N., Merkoçi, A., 2015. ACS Nano 9, 7296–7305.
Ohlsson, P.-I., Paul, K.-G., Sjöholm, I., 1977. J. Biol. Chem. 252, 8222–8228.
Palmiter, R.D., 1998. Proc. Natl. Acad. Sci. U.S.A. 95, 8428–8430.
Patra, S., Crespo, T.H., Permyakova, A., Sicard, C., Serre, C., Chaussé, A., Steunou, N., Legrand, L., 2015. J. Mater. Chem. B 3, 8983–8992.
Peroza, E.A., Schmucki, R., Ggntert, P., Freisinger, E., Zerbe, O., 2009. J. Mol. Biol. 87, 207–218.
Raj, C.R., Ohsaka, T., 2003. J. Electroanal. Chem. 540, 69–77.
Rissin, D.M., Kan, C.W., Campbell, T.G., Howes, S.C., Fournier, D.R., Song, L., Piech, T., Patel, P.P., Chang, L., Rivnak, A.J., Ferrell, E.P., Randall, J.D., Provuncher, G.K., Walt, D.R., Duffy, D.C., 2010. Nat. Biotechnol. 28, 595–600.
Wasserman, D.H., 2009. Am. J. Physiol. Endocrinol. Metab. 296, E11–E21.
Xianyu, Y., Wang, Z., Jiang, X., ACS Nano 8, 12741-12747.
Yetisen, A.K., Moreddu, R., Seifi, S., Jiang, N., Vega, K., Dong, X., Dong, J., Butt, H., Jakobi, M., Elsner, M., Koch, A.W., 2019. Angew. Chem. Int. Ed. 58, 10506–10513.
Yu, Q., Xue, L., Hiblot, J., Griss, R., Fabritz, S., Roux, C., Binz, P.-A., Haas, D., Okun, J.G., Johnsson, K., 2018. Science 361, 1122–1126.
Zarei, M., 2017. Biosens. Bioelectron. 98, 494–506.
Zhao, W., Ali, M.M., Aguirre, S.D., Brook, M.A., Li, Y., 2008. Anal. Chem. 80, 8431–8437.
Zhou, Z., Hartmann, M., 2013. Chem. Soc. Rev. 42, 3894–3912.
Zhu, Z., Guan, Z., Jia, S., Lei, Z., Lin, S., Zhang, H., Ma, Y., Tian, Z.-Q., Yang, C.J., 2014. Angew. Chem. Int. Ed. 53, 12503–12507.
Zhu, Z., Guan, Z., Liu, D., Jia, S., Li, J., Lei, Z., Lin, S., Ji, T., Tian, Z., Yang, C.J., 2015. Angew. Chem. Int. Ed. 54, 10448–10453.